

HARD AND SOFT X-RAY OBSERVATIONS OF OCCULTED AND NONOCCULTED SOLAR LIMB FLARES

JOHN T. MARISKA

E. O. Hulburt Center for Space Research, Code 7670, Naval Research Laboratory, Washington DC 20375-5352; mariska@aspen.nrl.navy.mil

AND

JAMES M. McTIERNAN

Space Sciences Laboratory, University of California at Berkeley, Berkeley, CA 94720

Received 1998 May 29; accepted 1998 October 26

ABSTRACT

Using observations from the *Yohkoh* Bragg Crystal Spectrometer (BCS), the Soft X-Ray Telescope, and the Hard X-Ray Telescope, we have examined the properties of 45 limb flares. Twenty-eight of the flares appear to have most or all of their footpoints occulted by the solar limb, leaving only soft X-ray emission from a looptop source visible. The remaining 17 flares have exposed footpoints. In most observational characteristics, occulted limb flares are indistinguishable from nonocculted limb flares. There does appear to be some evidence that the peak temperature observed in the BCS Ca XIX channel is lower by 2–3 MK in the occulted flares. We also see some tendency for the hard X-ray spectra averaged over the entire event to exhibit a softer spectral index in the occulted limb flares. Most of the flares for which it is possible to measure a peak in the Ca XIX nonthermal broadening velocity as a function of time show that the peak in the nonthermal broadening velocity occurs after the first significant hard X-ray peak.

Subject headings: Sun: flares — Sun: X-rays, gamma rays

1. INTRODUCTION

As a result of new observations made mostly with the instruments on the *Yohkoh* satellite, it appears that key events in the early phases of a solar flare take place above the loop or loops that eventually appear in soft X-rays. These observations have led to a refined picture of the impulsive phase (e.g., Tsuneta 1996; Aschwanden & Benz 1997) in which magnetic reconnection takes place well above the loops observed in soft X-rays. Acceleration of electrons then occurs in a cusp region beneath the reconnection site and above the loops seen in soft X-rays. This region has a relatively low density and hence should be weak in soft X-rays.

Shortly after the flare has begun, the bulk of the soft X-ray emission should originate in the loops that have already been heated by accelerated electrons and are now magnetically isolated from the reconnection region. At the earliest times in the impulsive phase, however, one might expect a more complex situation, in which heated plasma is rushing up field lines that are still connected to the precipitating electrons and there is no strong additional emission from the closed structures. At these early times, the dynamical properties of the soft X-ray-emitting plasma may reveal something about the nature of the heating process.

When they are imaged in soft X-rays, many disk and limb flares show a concentrated emission source at the assumed location of the loop top (e.g., Acton et al. 1992; Feldman et al. 1994). This source appears early in the flare and is thus probably related in some way to the other impulsive phase phenomena. Its existence at the top of an apparently thermal soft X-ray-emitting loop presents a challenge to the conceptual model outlined above.

Because these loop-top sources represent a challenge to existing models, it is important to obtain as much information about their physical properties as possible. Ratios of soft X-ray images taken with the Soft X-Ray Telescope (SXT) on *Yohkoh* can provide temperatures and emission

measures in these sources. These estimates, however, rely on the assumption that the plasma conditions are changing slowly in the time it takes to acquire a pair of images. Moreover, because they rely on ratioing images taken through broadband filters, the estimates require the use of extensive plasma emissivity calculations as well as accurately determined filter transmission curves. The Bragg crystal spectrometer (BCS) on *Yohkoh* provides high temporal and spectral resolution observations over selected wavelength bands that permit an alternative determination of the physical conditions in the flaring plasma. For most flares, useful data are available earlier in the impulsive phase than is the case with the SXT. Unfortunately, the BCS views the entire Sun, and thus for most flares it cannot isolate individual components of the flaring plasma. When a flare takes place at the solar limb, though, some parts of the flare may be behind the limb, permitting an examination of only the loop-top source.

Analyses of soft X-ray spectra from ions such as Ca XIX provide estimates of temperatures, emission measures, nonthermal broadening velocities, and bulk mass motions in the evolving flare plasma. Systematic study of these parameters for many flares have been undertaken using data from spectrometers on the *Solar Maximum Mission* (SMM), *P78-1*, *Hinotori*, and *Yohkoh* satellites. Doschek et al. (1986) provide a review of the SMM and *P78-1* observations and they issues they raise, Tanaka (1987) summarizes many of the *Hinotori* results, and Bentley (1996) reviews some of the major *Yohkoh* results.

The physical process that produces the observed nonthermal broadening has been a subject of considerable debate. Many investigators believe that it is associated with the Doppler shifts that are thought to be evidence for chromospheric evaporation early in a flare (e.g., Doschek et al. 1986). This view, however, has always suffered from nagging inconsistencies, such as the observation that the nonthermal broadening velocity is independent of the flare

position on the solar disk (e.g., Antonucci 1989; Mariska, Doschek, & Bentley 1993). This observation suggests that the nonthermal broadening velocity may instead be more directly related to the reconnection process that is thought to power the flare (e.g., Antonucci, Benna, & Somov 1996). Thus observing the characteristics of occulted and non-occulted limb flares may provide additional insights into the processes at work as the flare is initiated.

Khan et al. (1995) and Mariska, Sakao, & Bentley (1996) have examined *Yohkoh* BCS data for small numbers of occulted limb flares, producing conflicting conclusions. Khan et al. (1995) examined BCS observations of four occulted *GOES* class C5.4–C6.9 flares that occurred in a single active region over a period of about 10 hr. They concluded that there were no obvious differences between the temperatures and nonthermal velocities measured for those flares and the same quantities measured in disk flares with spectrometers flown on earlier satellites. Mariska et al. (1996) examined four occulted and four nonocculted flares. They found that most parameters measured with the BCS were similar between the two kinds of flares, except for the nonthermal broadening velocity, which was smaller for the occulted flares.

In this paper we extend the earlier study of Mariska et al. (1996) by examining a larger sample of occulted and non-occulted limb flares. The primary goal of this study is to determine whether the soft X-ray-emitting loop-top sources are similar to or different from the more uniform emission observed from the entire loop. This more uniform emission is usually considered to be a consequence of the heating produced by the thermalization of the accelerated particles at the loop footpoints.

2. DATA SELECTION

The observations used in this study were all obtained with the instruments on the Japanese *Yohkoh* spacecraft, which was launched in 1991 August and has been operating continuously since then. Ogawara et al. (1991) provide an overview of the entire mission. For this study we used observations from the BCS (described in detail by Culhane et al. [1991] and Lang et al. [1992]), the SXT (described in detail by Tsuneta et al. [1991]), and the Hard X-Ray Telescope (HXT; described in detail by Kosugi et al. [1991]).

From 1991 October 1 to 1996 October 31, the instruments on the *Yohkoh* satellite went into flare mode approximately 2600 times. Using a combination of the *Yohkoh* event logs and the SXT and BCS observing logs, we have compiled a list of all those events for which the solar radius vector of the center of the SXT partial frame images for the event had a value of 1.0 or greater and the peak total count rate observed in the BCS Ca XIX channel had a value greater than 500 s^{-1} . This procedure produced a list of 169 events. Using light curves in the BCS Fe XXV and Ca XIX channels, we reduced this initial list to 94 candidate limb flares that had reasonable BCS coverage of significant portions of the rise phase. For each of these candidate limb flares, we plotted light curves of the total count rate in each SXT filter and compared them with the light curves obtained with the BCS. This identified a small number of events where the SXT was observing a flare at the limb while the BCS was observing a stronger event at a different location on the Sun.

While a flare with an SXT partial frame center location with a solar radius vector of 1.0 or greater is at the limb, it is

not clear from that single number whether the footpoints of the flaring loop or loops are occulted or not. To make that determination, we relied on a combination of visual examination of the SXT partial frame images with the position of the solar limb added using spacecraft pointing information and data from the Space Environment Center (SEC) weekly flare reports, which provide $H\alpha$ positions for most flares. We were thus able to sort the flares into groups based on whether the SXT images showed emission concentrated only at or above the limb or included significant emission on the disk, and on whether the flare had $H\alpha$ emission associated with it at nearly the same limb location. Flares with SXT images showing concentrated emission only at or above the limb and with no $H\alpha$ emission were considered to be the most likely ones to have occulted footpoints. From the flares satisfying those criteria, we selected all those events for which enough useful data existed from the *Yohkoh* BCS and SXT for further analysis. Columns (1)–(5) of Table 1 list the key timing and positional information for those 28 occulted flares. The start and peak times for each flare and the *GOES* class are from the SEC weekly flare reports. The flare location is the position of the center of the SXT partial frame images for the flare. Since the images are normally centered on the brightest pixel, this provides an excellent position for the soft X-ray-emitting portion of the flare. These positions often differ by small amounts from the $H\alpha$ -based positions reported by the SEC.

Many flares in the initial list exhibited significant disk emission in SXT images and were observed in $H\alpha$ from the ground. From those flares we selected all the events for which enough useful data existed from the *Yohkoh* BCS and SXT for further analysis. Columns (1)–(5) of Table 2 list the key timing and positional information for those 17 non-occulted flares.

Another way to determine whether a flare has occulted or nonocculted footpoints is to construct hard X-ray images of the event using the *Yohkoh* HXT. If the images exhibit hard X-ray emission from footpoints on the disk, then it is reasonable to assume that the footpoints are not fully occulted. Unfortunately, many of the flares examined in this study are too weak for useful images to be synthesized. Thus for this study we have only used HXT data for determining the spectral index of the hard X-ray emission and for studying the relationship between changes in the nonthermal broadening observed with BCS and the hard X-ray emission.

Figure 1 shows examples of SXT data taken early in an occulted (1991 Dec 10) and a nonocculted (1992 Jul 17) flare. Both exposures are the earliest available properly exposed images taken in the thin Al filter. Most of the occulted flares look similar to the example shown. Usually the soft X-ray emission is concentrated right at or just above the solar limb, which is represented by the solid line in each panel. While there may be some emission from the flaring region on the disk, there are no strong, concentrated emitting features there suggesting loop footpoints. The non-occulted flares exhibit a wider range of emitting features. Generally, they are characterized by one or more strong emitting features on the disk. Often there are also strong emitting features above the limb, which appear to be looptop sources.

For each flare listed in Tables 1 and 2, we have processed the BCS Ca XIX spectral data to correct for instrumental effects and applied a wavelength calibration. In addition,

TABLE 1
 OCCULTED LIMB FLARE CHARACTERISTICS

DATE (1)	TIME (UT)		CLASS (4)	LOCATION (5)	T_{\max} (MK) (6)	EM_{\max} (cm^{-3}) (7)	ξ_{\max} (km s^{-1}) (8)	SXT SIZE		γ (11)	DELAY (s) (12)
	Start (2)	Peak (3)						50% (arcsec) (9)	25% (arcsec) (10)		
1991 Oct 12	23:52	23:58	C5.8	N22E90	14.6	0.069	168	13.9	19.1	9.1	31 ± 8
1991 Dec 10	03:59	04:04	C9.3	S15E90	15.0	0.085	138	9.7	18 ± 5
1992 Jan 13	18:59	19:13	M1.3	S10E90	15.0	0.13	147	18.5	31.6	9.5	>60
1992 Jul 4	22:44	22:51	C6.9	S12E89	15.7	0.065	98	9.9	13.5	9.3	>71
1992 Jul 18	05:05	05:11	C5.8	S14W88	14.2	0.055	139	13.8	17.7	9.4	-20 ± 12
1992 Aug 24	06:06	06:13	C2.5	N15W85	12.6	0.040	164	12.9	20.1	7.3	-131 ± 9
1992 Oct 27	20:50	20:55	C2.1	N08W90	12.6	0.025	152	28.8	36.3	...	>-65
1992 Oct 27	22:15	22:20	C5.4	N07W90	12.7	0.080	178	13.0	28.8	7.2	2 ± 14
1992 Oct 31	16:55	17:00	C2.5	S26W87	21.7	0.016	157	8.1	16.8	8.4	-15 ± 11
1992 Nov 5	06:17	06:22	M2.0	S17W88	16.5	0.25	175	10.1	14.0	5.8	-20 ± 3
1992 Nov 5	20:26	20:41	C8.2	S17W88	14.1	0.16	185	9.1	15.8	8.6	-36 ± 2
1992 Nov 24	09:59	10:05	C6.9	S06W89	19.3	0.10	156	18.5	26.1	7.1	>-30
1992 Nov 24	14:13	14:29	C5.9	S06W89	13.1	0.08	131	11.8	19.7	10.1	...
1992 Nov 24	15:47	16:04	C5.4	S06W89	15.2	0.055	145	11.3	17.2	10.3	-35 ± 33
1992 Nov 24	20:28	20:38	C6.4	S06W89	17.8	0.10	159	11.0	16.1	9.1	...
1993 Mar 15	09:58	10:03	C3.0	S04W90	12.6	0.041	153	22.0	35.2	5.6	>-18
1993 Mar 15	19:04	19:11	C5.5	S05W90	13.7	0.080	158	24.5	45.2	7.5	-23 ± 6
1993 Mar 23	23:47	23:55	C2.5	N16W87	14.1	0.038	149	13.7	30.0	10.9	-79 ± 12
1993 Mar 24	03:20	03:26	C6.6	N17W87	14.6	0.14	160	21.5	29.1	7.6	>-16
1993 May 25	01:12	01:16	C2.1	N14E84	13.1	0.031	173	9.4	12.8	8.1	-31 ± 11
1993 Sep 26	10:21	10:27	C3.4	N12E90	13.4	0.099	213	11.4	17.6	7.6	...
1993 Sep 26	18:26	18:31	C2.6	N12E90	13.9	0.03	176	13.3	18.1	...	-79 ± 12
1994 Jan 11	07:50	08:17	C1.7	N10W86	15.0	0.025	278	11.4	17.7	9.2	...
1994 Jan 15	09:25	09:30	C1.9	N05E89	13.7	0.022	152	15.9	30.1	6.3	-31 ± 14
1994 Feb 27	08:25	09:20	M2.8	N08W88	13.2	0.45	120	30.2	49.8	7.6	-48 ± 3
1995 Jan 29	17:42	17:51	C3.2	S12E90	12.3	0.071	146	8.2	12.9	7.1	>28
1995 Apr 22	03:57	04:32	C5.5	S00W90	13.7	0.08	119	12.6	20.0
1996 May 6	15:12	15:21	C2.5	S08E90	12.2	0.043	187	15.9	23.9	5.9	>-66

TABLE 2
 NONOCCULTED LIMB FLARE CHARACTERISTICS

DATE (1)	TIME (UT)		CLASS (4)	LOCATION (5)	T_{\max} (MK) (6)	EM_{\max} (cm^{-3}) (7)	ξ_{\max} (km s^{-1}) (8)	SXT SIZE		γ (11)	DELAY (s) (12)
	Start (2)	Peak (3)						50% (arcsec) (9)	25% (arcsec) (10)		
1991 Dec 9	18:53	18:56	M1.1	S06E85	14.1	0.15	181	8.8	29.8	7.5	>11
1992 Jan 13	17:23	17:34	M2.0	S15W90	19.0	0.21	131	32.8	41.7	6.6	87 ± 8
1992 Feb 19	03:34	03:55	M3.7	N04E89	19.0	0.50	163	20.2	26.8	9.1	-26 ± 2
1992 Feb 26	01:33	01:39	M1.3	S15W90	17.4	0.19	196	15.1	20.7	7.7	7 ± 12
1992 Jul 5	17:53	18:01	C8.6	S11E89	14.8	0.11	126	52.6	60.1	9.2	7 ± 12
1992 Jul 5	19:56	20:00	M1.1	S13E86	18.0	0.15	114	11.1	21.2	8.7	-4 ± 2
1992 Jul 17	22:33	22:41	C5.3	S11W87	14.5	0.07	150	30.3	36.3	6.5	>-89
1992 Aug 24	01:10	01:15	C2.2	N14W90	13.7	0.028	189	38.0	46.6	8.1	-28 ± 12
1992 Sep 9	01:53	02:13	M3.1	S11W87	16.0	0.30	160	11.4	26.0	8.4	-13 ± 3
1992 Oct 4	22:11	22:27	M2.4	S08W83	16.0	0.30	116	6.3	10.3	4.9	-50 ± 6
1992 Oct 12	21:48	21:53	C2.5	S16W88	16.0	0.023	122	8.6	12.4	6.3	-70 ± 6
1993 Jan 2	23:37	23:52	C8.4	S09W87	12.5	0.12	132	14.9	25.0	4.8	-41 ± 36
1993 Feb 1	09:58	10:05	C6.9	S11E90	14.5	0.090	155	10.9	25.3	8.0	...
1993 Mar 2	14:58	15:10	C5.0	S02E90	17.0	0.055	190	40.4	45.6	6.6	-171 ± 36
1993 Mar 24	01:39	01:43	C3.1	N16W87	13.6	0.050	153	11.7	22.2	7.7	>-39
1993 Sep 27	12:04	12:12	M1.8	N08E90	14.5	0.30	201	16.8	24.6	6.8	>8
1995 Jan 30	01:08	01:17	C2.8	S12E85	13.0	0.35	135	12.1	17.7	...	-10 ± 9

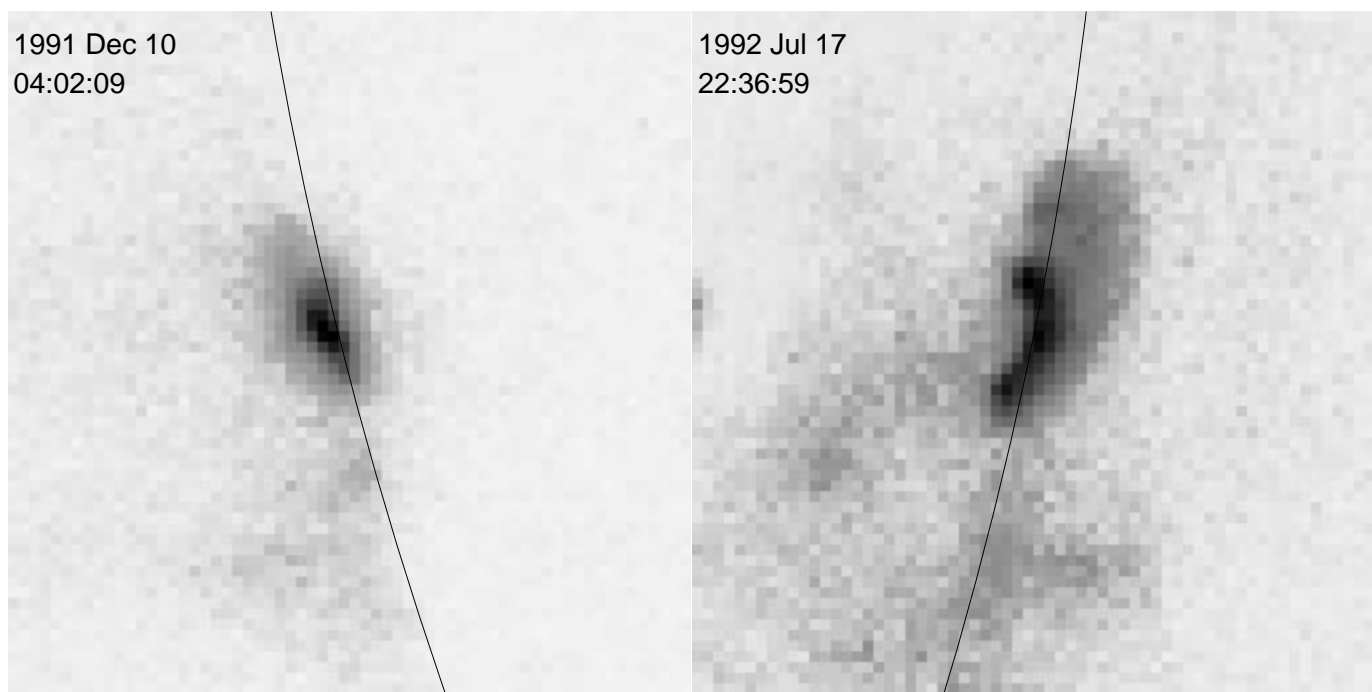


FIG. 1.—SXT thin Al images of an occulted flare (1991 Dec 10) and a nonocculted flare (1992 Jul 17). The solid line on each image marks the location of the solar limb.

the data were accumulated until the total number of counts in the Ca XIX channel exceeded 8000. This assures that each spectrum contains sufficient detail for spectral fitting software to work successfully.

3. ANALYSIS

Since all the flares listed in Tables 1 and 2 are at the limb, we expect that any heating-driven flows present early in the flare will be predominately transverse to the line of sight. Thus we do not expect any Doppler-shifted components in the soft X-ray line profiles. This expectation is borne out by visual inspection of the BCS Ca XIX line profiles early in each flare. We have, therefore, fitted the Ca XIX spectra for each flare listed in Table 1 using a single-component isothermal model. Each Ca XIX spectrum is thus characterized by a temperature T , an emission measure EM, and nonthermal broadening ξ .

These parameters were determined using standard spectral fitting techniques. For each observed spectrum, a synthetic Ca XIX spectrum was computed, and the fitting parameters for it were varied to locate a minimum in the computed χ^2 . The synthetic spectra primarily use atomic data computed by Bely-Dubau et al. (1982), with some minor modifications in wavelengths and excitation rates (G. A. Doschek 1994, private communication).

Figures 2a and 2b show the time histories of the physical parameters derived from the BCS Ca XIX spectra obtained during the two flares shown in Figure 1. The top portion of each figure shows the total count rate in the Ca XIX channel at the time cadence of the actual observations, while the remaining plots show the values of the fitting parameters obtained from the time-integrated spectra. Note that for both these events the BCS data are available earlier than the first useful image from SXT. This is due to the added time that the SXT requires after a flare flag occurs to locate

a flare and begin taking higher time-cadence data. Thus the BCS data represent a powerful probe of the earliest times in a flare.

To reduce clutter, we have not included error bars on the plots. Generally, the spectral fits have reduced χ^2 values of less than 3, with the majority falling between 1 and 2. Profiles with reduced χ^2 values greater than 2 usually show small amounts of excess emission in both the blue and red wings of the Ca XIX resonance line or occasionally an instrumental spike on the line profile, which has not been removed. Attempts to fit this excess emission with a second broader Gaussian component generally do not result in a converged solution. Assuming that the variation of each fitting parameter is independent of the values of the other fitting parameters near the values that yield the best fit to the data, the formal error for each fitting parameter is the square root of the corresponding element in the covariance matrix produced by the fitting procedure. The average error in the EM estimates ranges from less than 10% for the stronger flares to as high as 30% for the weakest flares. For most of the flares in this study, the errors in T are $\lesssim(6-8) \times 10^5$ K and those for ξ are $\lesssim 3-8$ km s $^{-1}$.

The physical variables for both flares show the same basic behavior. While the count rate in the Ca XIX channel peaks and decays, the emission measure derived from the Ca XIX spectra generally either rises continuously until well past the peak in the Ca XIX count rate or reaches a nearly constant value until well after the Ca XIX peak. During the rise phase of the flare in Ca XIX, the temperature also rises. It usually peaks near the peak in Ca XIX emission and then decays with the decaying emission. Early in the flare, the nonthermal broadening velocity is at or near its peak value for the event. It then generally declines throughout the flare. Even when ξ rises for a short time early in the flare, it peaks well before the Ca XIX temperature maximum.

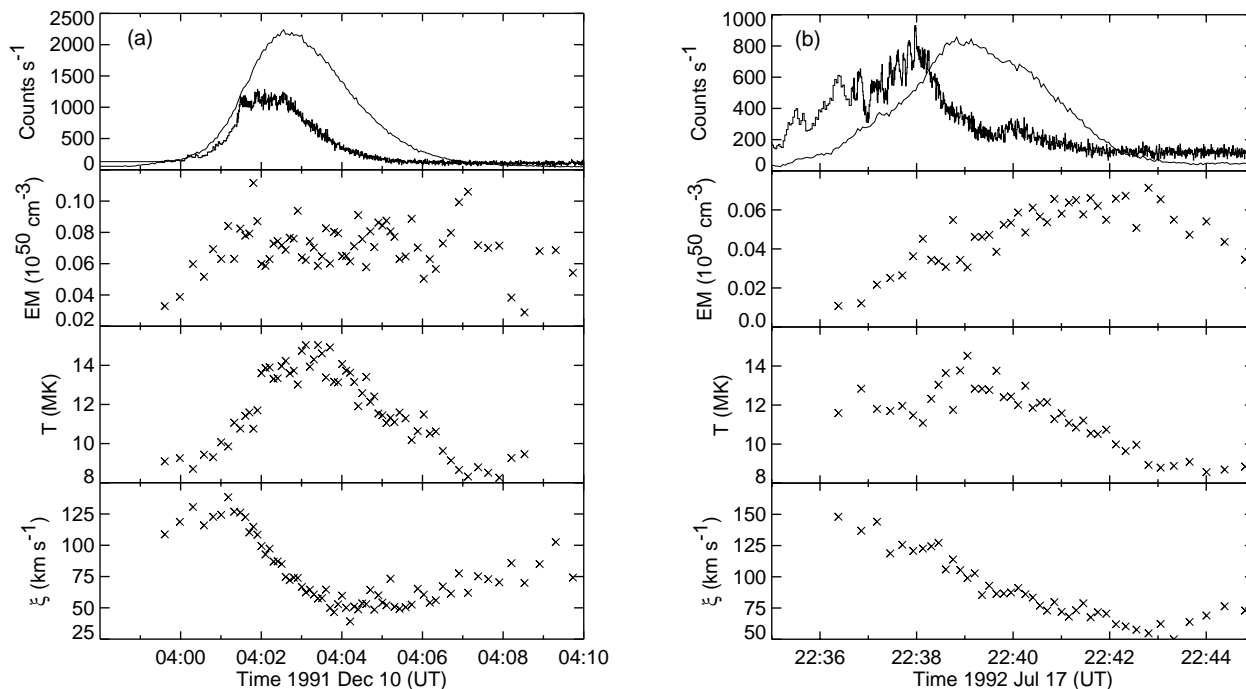


FIG. 2.—Time history of the total count rate in the BCS Ca XIX channel and the derived physical variables for (a) the occulted flare and (b) the nonoccluded flare, both shown in Fig. 1. Also plotted as histograms on the top panels are the HXT L channel count rates per subcollimator scaled by a factor of 100.

It may at first appear inconsistent for the count rate in the Ca XIX channel to peak and decay while the Ca XIX EM remains constant or rises. This is the result of the temperature dependence of the emissivity of the Ca XIX lines, which rises steeply with increasing temperature throughout the temperature range plotted on the figures. Thus, even though the count rate in the Ca XIX channel is declining, the observed decrease in the temperature requires an increasing emission measure to produce the observed line emission.

We are interested here in determining if there are any differences between occulted and nonoccluded flares. Thus, instead of performing a detailed analysis of the time histories of the physical variables computed for each flare, we have characterized each one by determining the maxima in the measured quantities. These maxima are listed for each flare in Tables 1 and 2. Comparisons among the results presented in the tables can be made in a number of ways. Although the number of flares we have analyzed is relatively modest, plotting the results as normalized histograms can be an effective way to look for differences between the two data sets.

Figure 3 shows normalized histograms of the frequency of occurrence of the peak temperature for each flare listed in Tables 1 and 2. To construct this histogram the data have been grouped in 2 MK bins. While the number of flares in the two samples is small, the histograms do appear to show a tendency for the nonoccluded flares to have a peak temperature that is higher on average than the occulted flares. Moreover, the distribution of peak temperatures appears to be broader for the nonoccluded flares.

Determining whether the tendency shown in the histograms is a real effect is complicated by additional factors. Feldman et al. (1995, 1996) have shown that there is a correlation between the flux measured with *GOES* and the temperature measured with the BCS at the maximum count

rate for the selected channel. Thus, if there were a larger number of strong flares in the nonoccluded sample, we might expect the nonoccluded temperature histogram to peak at a higher temperature. To examine that possibility, we have plotted in Figure 4 the normalized histograms of the *GOES* class for the two flare groups. The histograms suggest that the sample of occulted flares have fewer strong flares than the sample of nonoccluded flares.

This may be misleading, though. Measurements of the peak flux with *GOES* for occulted flares are probably not a true measure of the magnitude of the actual flare. Since the flare is partially occulted by the solar limb, its true peak soft X-ray flux must be larger than the value measured with *GOES*. In other words, the histogram for the *GOES* class of the occulted flares in Figure 4 probably needs to be shifted to higher *GOES* fluxes. Thus we believe that the tem-

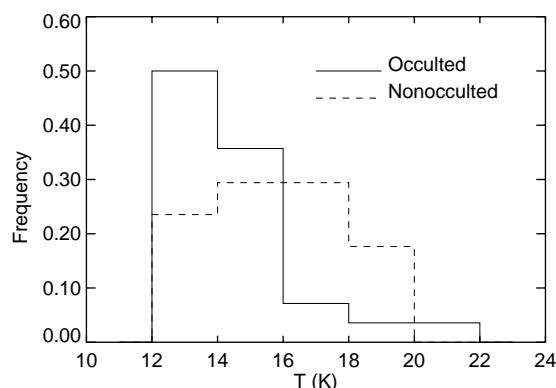


FIG. 3.—Normalized histograms of the peak temperature measured in the BCS Ca XIX channel for each flare listed in Tables 1 and 2.

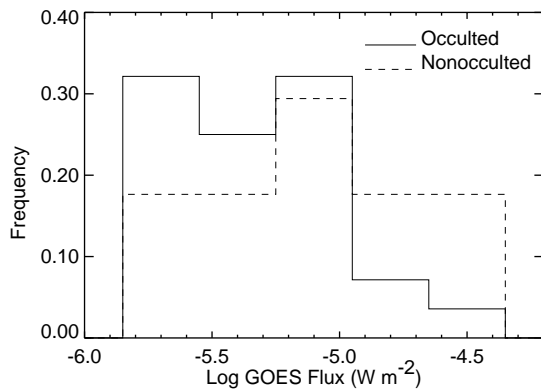


FIG. 4.—Normalized histograms of the *GOES* flux measured for each flare listed in Tables 1 and 2. A flux of 10^{-6} W m^{-2} corresponds to a *GOES* class of C1.

perature effect shown in Figure 3 is real and that the occulted flares do appear to show a tendency for the peak temperature to be lower than those of the nonocculted flares.

Figure 5 shows normalized histograms of the frequency of occurrence of the peak nonthermal broadening, ξ , for each flare listed in Tables 1 and 2. Both histograms peak at the same velocity, between 150 and 175 km s^{-1} . While the distribution of nonthermal broadening velocities shows some tendency to be slightly wider for the nonocculted flares, there is no clear evidence for any differences between them and the occulted flares. Mariska et al. (1993) and Mariska (1994) have shown that there is no correlation between the *GOES* class of a flare and the nonthermal broadening. Thus this result is not subject to the ambiguity that clouds any attempt to determine whether the peak temperature in an occulted flare differs from that measured in a similar nonocculted flare.

Since the *Yohkoh* BCS is uncollimated, the nonthermal broadening can be influenced by the size of the emitting source. The orientation of the BCS crystals is such that only the extent of the emitting region in the north-south direction contributes to the broadening. For the Ca XIX channel, this contribution to the broadening amounts to 1.1 km s^{-1}

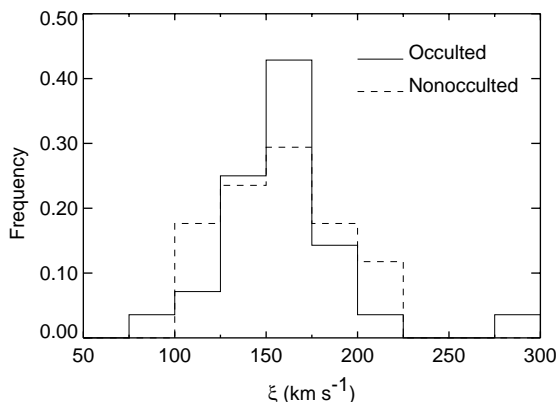


FIG. 5.—Normalized histograms of the peak nonthermal broadening velocity measured in the BCS Ca XIX channel for each flare listed in Tables 1 and 2.

arcsec^{-1} (e.g., Mariska 1994). Thus substantial differences in size in the north-south direction between occulted and nonocculted flares could influence the deduced nonthermal broadening measurements.

To examine the influence of this effect on our measured nonthermal broadening velocities, we have measured the north-south extent of each flare in our sample using an SXT partial frame image taken through the Be filter. This filter most closely approximates the temperature range of the emission that is normally measured in the BCS Ca XIX channel (e.g., Tsuneta et al. 1991). Since the nonthermal broadening peaks early in the flare, we use the earliest available SXT partial frame image in the Be filter. For each flare, we measured the north-south extent of the 50% and 25% contours in the image. Those measurements (in arcseconds) are listed in Tables 1 and 2.

Figure 6 shows normalized histograms for the north-south extent in km s^{-1} of each flare at the 50% level. While there is some indication that more nonocculted flares occupy the higher velocity bins, it is clear that most of the occulted and nonocculted flares are of comparable size. Thus we believe that the similarity of the magnitudes of the peak in the nonthermal broadening in the occulted and nonocculted flares is not being significantly influenced by size differences between the two classes of flares.

Since a mostly occulted flare should have only a small region emitting at the temperature of formation of the emission from the BCS Ca XIX channel, we would expect that the nonocculted flares would generally be larger than the occulted flares. For many flares on the disk, however, there is often only one strong soft X-ray-emitting source, especially in images taken with the SXT Be filter. Thus it is not surprising that the sizes in km (corrected for the variation in the size of the Sun with date) are comparable for most of the occulted and nonocculted flares in our study, with only a few of the nonocculted flares being larger. This result may also be partly a selection effect. Flares that have complex emitting structures on the disk, such as multiple strong foot-point sources, tend to be larger and would be excluded from this study because of instrumental problems with the BCS at high count rates.

While many of the flares are too weak to construct images using the *Yohkoh* HXT data, we have made power-

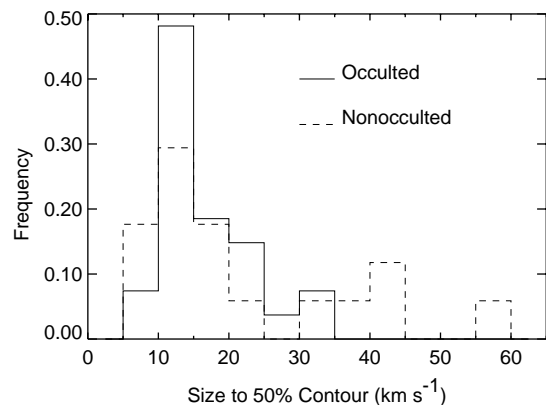


FIG. 6.—Normalized histograms of the extent in the north-south direction of the 50% intensity contour measured with the SXT through the Be filter. The sizes have been converted to units of km s^{-1} for comparison with the BCS Ca XIX channel spectra.

law fits to the data. To characterize each flare in hard X-rays, we have performed power-law and thermal fits to the HXT data for both the entire flare and for smaller time intervals within the flare. The entire flare was defined as either the time interval that included all the data points in the HXT L channel (14–23 keV) that were at least a factor of 2 above the background level or all the data points in the HXT M1 channel (23–33 keV) that were at least a factor of 2 above the background level. In the first case, the fit included all the HXT energy channels with useful data. In the second case, the HXT L channel was excluded. Because many of the flares in this study were relatively weak, only the fits using the HXT L channel could be performed on the majority of the flares. Thus, in Tables 1 and 2 we list the resulting values of the power-law index γ for the entire flare defined using the HXT L channel definition. Generally, for those cases in which we have power-law fits that begin at the energy of the HXT M1 channel, the power-law indices are comparable to those determined beginning with the L channel.

Mariska et al. (1996) found in the limited number of flares that they examined that the occulted flares tended to have power-law indices that were larger than the nonocculted flares. They interpreted this as evidence that the hard X-ray emission in the occulted flares was coming from a thin-target source in the upper portions of the flaring loop or loops rather than from a thick-target source at the loop footpoints. In our larger data set, the average value of γ for the occulted flares is 8.2 ± 1.5 , while for the nonocculted flares it is 7.3 ± 1.3 . Thus we cannot conclusively say that, when the hard X-ray burst data for each flare are considered in their entirety, the occulted flares are softer.

Figure 7 shows normalized histograms of the values of γ listed in Tables 1 and 2. The distributions do show some evidence of a separation between the occulted and nonocculted flares. For example, 44% of the nonocculted flares have a value of γ smaller than 7, while only 14% of the occulted flares fall at these small values. The averages listed above, however, argue that the distributions are nearly the same.

Generally, when the first usable BCS spectra are obtained early in a flare, the nonthermal broadening velocity is large. Often the first usable spectrum shows the maximum value for ξ . In particle beam heating models, upflowing soft X-ray-emitting plasma should be a consequence of the beam

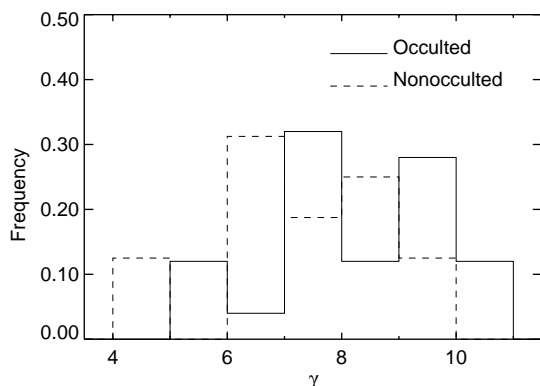


FIG. 7.—Normalized histograms of the measured values of the hard X-ray spectral index γ for each flare listed in Tables 1 and 2.

thermalization. If the enhanced nonthermal broadening is a consequence of this thermalization, then one would expect to see significant hard X-ray emission before the peak in ξ .

Recently, Alexander et al. (1998) have examined the relationship between the time of the maximum in the nonthermal broadening measured with the BCS Ca XIX and S XV channels and the time of the first significant hard X-ray peak observed with the HXT. They found that the maximum in ξ occurs before the first significant hard X-ray peak or that ξ is already declining from an apparently unobserved maximum when the first hard X-ray peak occurs. In our much larger sample of limb flares, we see both kinds of behavior. For example, the flare shown in Figure 2a shows a distinct peak in ξ that occurs before the first significant peak in HXT emission. On the other hand, the flare shown in Figure 2b exhibits a maximum in ξ before the first measurable spectrum. Thus, even though the hard X-ray burst occurs before this time, it is impossible to determine what the relationship is between the time of the peak in ξ and that time, except to say that the data are not inconsistent with the peak in ξ occurring before the first significant hard X-ray peak.

If we consider only those cases for which there is good hard X-ray coverage of the flare, then there are four possible relationships between ξ and the first significant peak in hard X-rays: (1) The nonthermal broadening shows a measurable increase to a maximum and that maximum occurs before the first significant hard X-ray peak. (2) The nonthermal broadening shows a measurable increase to a maximum, and that maximum occurs after the first significant hard

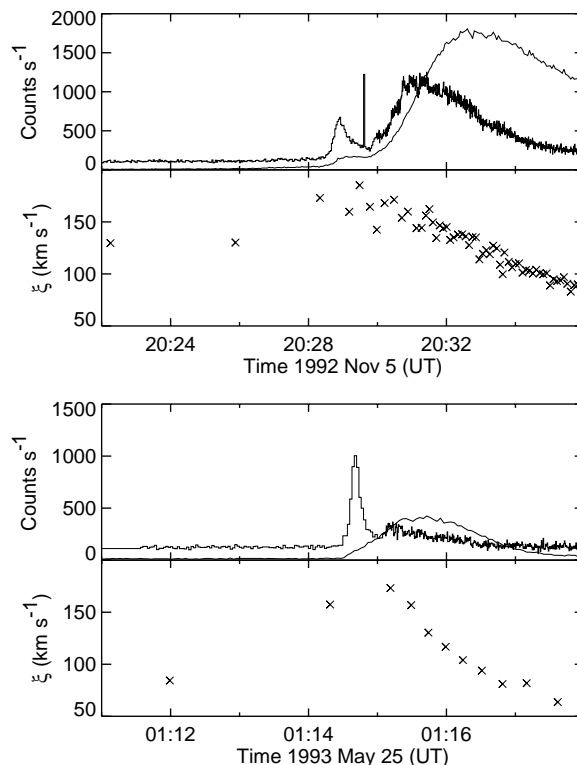


FIG. 8.—Time histories of the total count rate in the BCS Ca XIX channel (solid line), the HXT L channel count rate per subcollimator scaled by a factor of 100 (histogram), and the derived nonthermal line broadening velocities for two of the flares in our sample that exhibit a peak in ξ after the first peak in hard X-rays.

X-ray peak. (3) The nonthermal broadening is at its peak value in the first measurable spectrum, and that value occurs before the first significant hard X-ray peak. (4) The nonthermal broadening is at its peak value in the first measurable spectrum, and that value occurs after the first significant hard X-ray peak. Only relationships 1 and 3 are unambiguous evidence for the peak in ζ preceding the first significant hard X-ray peak.

For all the flares in our study for which the data are complete enough, we have computed the difference in s between the time of the first significant peak in hard X-rays measured in the HXT L channel and the peak in ζ measured in the BCS Ca XIX channel. These delays are listed in the last column of Tables 1 and 2. Relationships 1 and 2 appear in the tables as positive numbers with \pm ranges indicated. Those ranges are the result of the finite—and often large—integration times needed early in a flare to accumulate a statistically meaningful spectrum. Relationship 3 appears in the tables as a delay that is greater than a positive number, and relationship 4 appears as a delay that is greater than a negative number. Thus if the delay is negative, the peak in ζ occurred after the first significant peak in hard X-rays.

Because many of the flares are relatively weak, many of the results are only limits, all of which do not disagree with the possibility that the peak in ζ could take place before the first significant peak in hard X-rays. It is more interesting, however, to focus on the flares for which a peak time was determined for ζ . Figure 8 shows two examples of flares for which we can determine that time. In both cases, there is evidence for hard X-ray emission before the nonthermal broadening reaches a peak. The data for these two flares, which are typical of the ones we observed, show how challenging it is to make this kind of measurement. Generally, early in the flare when the nonthermal broadening is largest, the integration times are long, leading to relatively few measurements. Thus it is often difficult to unambiguously determine when the peak occurs in the nonthermal broadening.

For the 27 flares in the two tables for which we can measure a delay, we find that 21 have negative delays and only 6 have positive delays. Thus, for most of the flares for which we can measure the actual peak in ζ in the Ca XIX channel, that peak occurs after the first significant peak in hard X-rays. Even if we also include those flares for which the delay is clearly positive, then we still must conclude that the peak in ζ is usually after the first significant peak in hard X-rays.

4. DISCUSSION AND CONCLUSIONS

We have found that, based on a much larger sample than earlier studies, in most observational characteristics, occulted limb flares are indistinguishable from nonocculted limb flares. In particular, we do not see the tendency noted by Mariska et al. (1996) for occulted limb flares to have smaller peak values of the nonthermal line broadening than nonocculted limb flares. There does appear to be some evidence that the peak temperature observed in the BCS Ca XIX channel is lower by 2–3 MK in the occulted limb flares. We also see some tendency for the hard X-ray spectra averaged over the entire event to exhibit a slightly softer spectral index.

As we pointed out earlier, it is not possible to argue unambiguously that the reduction in peak temperatures we see in the occulted limb flares compared with the non-

occulted limb flares is a real effect. If it is a real effect, then does the temperature difference reveal anything about the nature of the energy deposition taking place early in a flare? Tsuneta (1996) and Tsuneta et al. (1997) have outlined a model for the structure and dynamics of the reconnection region that they assume powers a flare. In this model, the reconnection site sits well above the flare loops observed in soft X-rays and has both high- and low-temperature regions associated with it. High-temperature ridges mark the reconnected field lines. Between the ridges lies a cooler channel associated with the reconnection outflow. This cool channel lies below the reconnection site and above the normally observed soft X-ray-emitting loops. Tsuneta et al. (1997) argue based on SXT and HXT observations that the emission measure is larger in the cool channel than in the high-temperature ridges.

Unfortunately, the signal from both the high-temperature ridges and the cool channel is much weaker than that from the plasma that is filling the reconnected loops in response to the energetic particle heating. Thus, if any of those loops are exposed in the occulted limb flares, their emission should dominate the signal observed by the BCS. Since that is likely to be the case for all but the most extreme occultation geometries, we do not believe that our observations are probing the hot-ridge or cool-channel plasma. If an individual flare is exhibiting only those two regions, though, the reduced temperatures we see in the occulted limb flares are consistent with the picture outlined above.

Instead, in the occulted limb flares we are probably probing the looptop soft X-ray source. Forbes & Acton (1996) suggest that this material is created as a result of a thermal instability downstream from the termination shock associated with the downward jet from the reconnection region. They point out, however, that the existence of this feature depends on the plasma density, with low-density loops unable to produce the condensation. If we are indeed seeing this feature in some of the occulted limb flares, then our observations suggest that the temperature in the feature is roughly 2–3 MK less than that in the loops filling with plasma as a result of the energetic particle heating.

A number of observations have been reported of hard X-ray emission from occulted limb flares, usually stereoscopic observations from two spacecraft (e.g., Frost & Dennis 1971; Hudson 1978; Kane et al. 1979, 1992; Kane 1983). Both softer hard X-ray spectra (e.g., Kane et al. 1979) and harder hard X-ray spectra (e.g., Frost & Dennis 1971) have been reported for flares in which the footpoints were occulted. In a simple flaring loop model in which the footpoint hard X-ray emission is from a thick target and the looptop source is from a thin target, occulted flares should have a steeper spectrum (Brown, Hayward, & Spicer 1981). Our observations are roughly consistent with that picture.

Since our spectral indices include data from the HXT L channel (14–23 keV), some of the emission may be thermal in origin. This appears to be more of a problem for the nonocculted limb flares, which in the L channel frequently show the often-described spikey hard X-ray features superimposed on a more gradually varying component. Figure 9 illustrates this behavior. Both flares have roughly the same peak count rates in the HXT L channel, yet the nonocculted flare clearly shows a substantial gradual component probably due to thermal emission. The occulted flare also has a gradual component, but early in the event it is much weaker relative to the spikes. The absence of much of this gradually

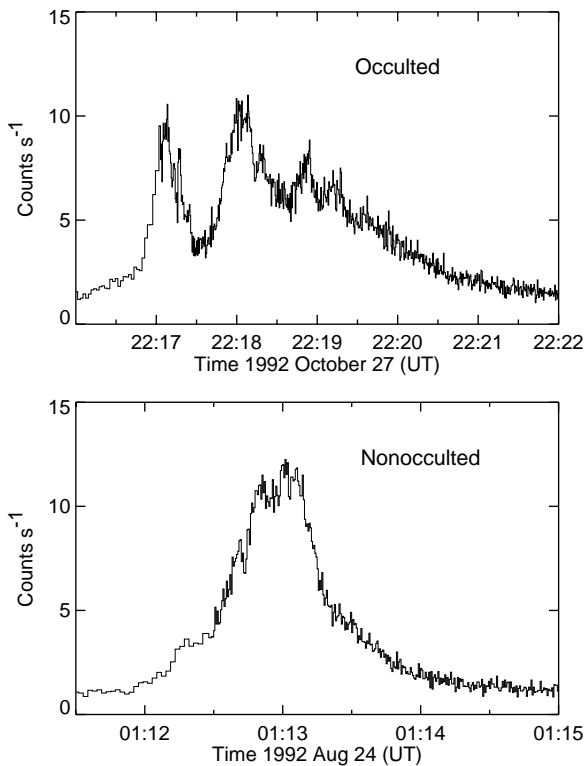


FIG. 9.—Time histories of the HXT L channel count rate per subcollimator for occulted and nonocculted flares with roughly the same peak count rates.

varying component in many of the occulted limb flares suggests that in those cases we are probably observing non-thermal emission.

For those flares for which there is considerable thermal emission in the HXT L channel, the power-law index we

obtain may be different from the true nonthermal power-law index. If the emission was purely thermal, higher temperatures would lead to smaller values of γ . Thus the tendency displayed in Figure 7 for nonocculted flares to have smaller values of γ is consistent with the tendency shown in Figure 3 for nonocculted flares to have higher temperatures.

Our observation that most of the flares for which we can make the measurement show that the first peak in hard X-ray emission precedes the peak in ζ differs from the result of Alexander et al. (1998). It should be noted, however, that their conclusion relies more heavily on observations in the BCS S xv channel, whereas ours relies only on BCS Ca xix data. Because the S xv channel is sensitive to much cooler plasmas, it often shows measurable spectra earlier in the flare than the Ca xix channel. It may be possible that ζ measured in the S xv channel peaks before ζ measured in the Ca xix channel. That would be opposite to the usual trends observed in the BCS soft X-ray channels, however. Generally, the emission from lines formed at higher temperatures rises faster and peaks earlier in a flare.

Now that the new solar cycle has produced significant numbers of flaring active regions, it may be possible to use data from multiple spacecraft to refine this picture. Imaging observations from the EIT experiment on *SOHO* and the recently launched *TRACE* satellite may provide more details on the morphology of occulted limb flares to help interpret the data from the still-operating BCS.

We thank the referee for valuable comments that helped improve the paper. This work was partially supported by a Supporting Research and Technology grant from the NASA Sun-Earth Connections Theme. *Yohkoh* data analysis at the University of California at Berkeley is supported by NASA Grant NAGW-5126 and Lockheed Subcontract SA30G4740R.

REFERENCES

- Acton, L. W., et al. 1992, *PASJ*, 44, L71
 Alexander, D., Harra-Murnion, L. K., Khan, J. I., & Matthews, S. A. 1998, *ApJ*, 494, L235
 Antonucci, E. 1989, *Sol. Phys.*, 78, 107
 Antonucci, E., Benna, C., & Somov, B. V. 1996, *ApJ*, 456, 833
 Aschwanden, M. J., & Benz, A. O. 1997, *ApJ*, 480, 825
 Bely-Dubau, F., et al. 1982, *MNRAS*, 201, 1155
 Bentley, R. D. 1996, in *Magnetodynamic Phenomena in the Solar Atmosphere: Prototypes of Stellar Magnetic Activity*, ed. Y. Uchida, T. Kosugi, & H. S. Hudson (Dordrecht: Kluwer), 177
 Brown, J. C., Hayward, J., & Spicer, D. S. 1981, *ApJ*, 245, L91
 Culhane, J. L., et al. 1991, *Sol. Phys.*, 136, 89
 Doschek, G. A., et al. 1986, in *Energetic Phenomena on the Sun*, ed. M. Kundu & B. Woodgate (NASA CP: 2439), 4-1
 Feldman, U., Doschek, G. A., Behring, W. E., & Phillips, K. J. H. 1996, *ApJ*, 460, 1034
 Feldman, U., Doschek, G. A., Mariska, J. T., & Brown, C. M. 1995, *ApJ*, 450, 441
 Feldman, U., Seely, J. F., Doschek, G. A., Strong, K. T., Acton, L. W., Uchida, Y., & Tsuneta, S. 1994, *ApJ*, 224, 235
 Forbes, T. G., & Acton, L. W. 1996, *ApJ*, 459, 330
 Frost, K. J., & Dennis, B. R. 1971, *ApJ*, 165, 655
 Hudson, H. S. 1978, *ApJ*, 224, 235
 Kane, S. R. 1983, *Sol. Phys.*, 86, 355
 Kane, S. R., Anderson, K. A., Evans, W. D., Klebesadel, R. W., & Laros, J. 1979, *ApJ*, 233, L151
 Kane, S. R., McTiernan, J., Loran, J., Fenimore, E. E., Klebesadel, R. W., & Laros, J. G. 1992, *ApJ*, 390, 687
 Khan, J. I., Harra-Murnion, L. K., Hudson, H. S., Lemen, J. R., & Sterling, A. C. 1995, *ApJ*, 452, L153
 Kosugi, T., et al. 1991, *Sol. Phys.*, 136, 17
 Lang, J., et al. 1992, *PASJ*, 44, L55
 Mariska, J. T. 1994, *ApJ*, 434, 756
 Mariska, J. T., Doschek, G. A., & Bentley, R. D. 1993, *ApJ*, 419, 418
 Mariska, J. T., Sakao, T., & Bentley, R. D. 1996, *ApJ*, 459, 815
 Ogawara, Y., et al. 1991, *Sol. Phys.*, 136, 1
 Tanaka, K. 1987, *PASJ*, 39, 1
 Tsuneta, S. 1996, *ApJ*, 456, 840
 Tsuneta, S., Masuda, S., Kosugi, T., & Sato, J. 1997, *ApJ*, 478, 787
 Tsuneta, S., et al. 1991, *Sol. Phys.*, 136, 37